Journal of Materials Chemistry A

Accepted Manuscript

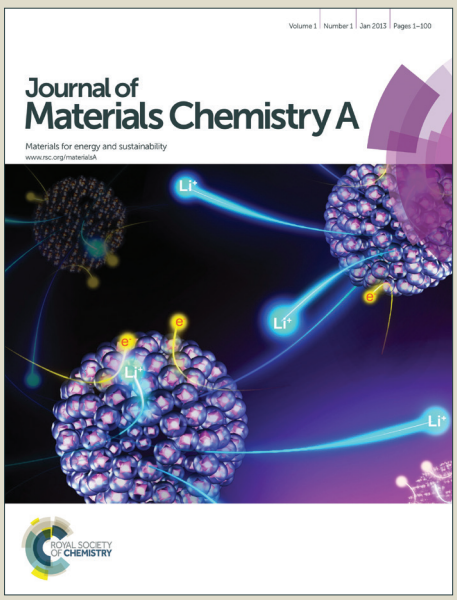

ROYAL SOCIETY OF CHEMISTRY

www.rsc.org/materialsA

Energy Harvesting and Storage Devices Fused into Various Patterns

*Hao Sun, Yishu Jiang, Longbin Qiu, Xiao You, Jiahua Yang, Xuemei Fu, Peining Chen, Guozhen Guan, Zhibin Yang, Xuemei Sun, Huisheng Peng**

State Key Laboratory of Molecular Engineering of Polymers, Collaborative Innovation Center of Polymers and Polymer Composite Materials, Department of Macromolecular Science and Laboratory of Advanced Materials, Fudan University, Shanghai 200438, China; E-mail: penghs@fudan.edu.cn.

Abstract: The conventional connection of energy devices by electrically conducting wires is less efficient and inconvenient, even unavailable in many applications. A general and effective method is here developed to connect energy harvesting or/and storage devices by simply stacking and gently pressing them. The energy devices are touched together and then rapidly fused into one by incorporating electrically conducting carbon nanotube sheet and self-healing polymer into a laddered structure. Flexible supercapacitors, perovskite solar cells and their integrated devices are demonstrated. Supercapacitors are fused into various patterns with tunable capacitances, perovskite solar cells are fused into one in series with linearly increasing output voltages, and supercapacitors and perovskite solar cells are also fused into an integrated device to simultaneously realize energy conversion and storage.

Energy harvesting and storage devices are widely used to power various electronic products in our life,[1-6] and they are generally connected in series or parallel by a large number of electrically conducting wires to output voltages or currents.[7] As a result, a complex fabrication is typically required to assemble them together with low efficiency while high cost. The introduced many conducting wires further bring a severe safety problem due to the short circuit, particularly, in the booming portable and wearable electronics. Flexible power systems are also needed by a broad spectrum of applications besides the portable and wearable electronic facilities, but the complex connection may make the assembled power system rigid although all building energy units are flexible. Therefore, it is necessary to find new methods to connect many energy devices more efficiently.

Interestingly, Google launched a revolutionary modular smartphone project named "Ara" to assemble a smartphone from standardized modules in early 2015, allowing for a high customisation and longer lifetime (Figure S1 and related references). The modular design is believed to be a mainstream in the future electronics. Similarly, it is

critical while unavailable to assemble energy device modules into a continuous power system without the use of external conducting wires.

Such fusible energy devices are herein developed by designing electrically conducting carbon nanotube (CNT) sheet and self-healing polymer (SHP) into a laddered structure and standardized module. The CNT sheet and laddered structure make the fusible energy devices available to be connected in series or parallel, and the SHP layer fuses them into the patterned structure. The energy device units can be fabricated into standardized modules and connected with each other at edges to form a continuous film, number or letter and even more complex pattern. Flexible supercapacitors and perovskite solar cells that have recently attracted increasing attentions are studied as demonstrations. High electrochemical storage and photovoltaic performances are well maintained for the fused device even under bending. These fusible energy devices can be produced for flexible powering systems at a large scale.

The fusible energy device units had been made from mechanically and electrically healable electrodes which were composed of aligned CNT sheet and SHP. The CNT sheet was dry-drawn from a spinnable CNT array that had been synthesized by chemical vapor deposition.[8,9] Many CNT sheets were cross-stacked onto a SHP film in favor of fusions in both transverse and longitudinal directions (Figure 1a). Some CNTs were embedded into the SHP film after a pressing treatment (Figure 1b). As expected, the SHP layer could be healed after breaking, so small composite films were fused into a continuous larger one. As the aligned CNT sheet showed a high optical transmittance (over 80% at the range of the visible light),[9] the resulting composite film was transparent with the underlying symbols clearly observed (inserted image in Figure 1c). The composite film was thin and could float on water (Figure S4).

The self-healing ability of the SHP layer was important in fusing the energy devices at edges. The fusing process of two aligned CNT/SHP films was completed in ~15 seconds at room temperature (Figure 1d-f). The gap between the two composite films disappeared after the fusion by the generation of hydrogen bonds in the SHP. The morphology evolution of the "scar" during the fusing process had been also verified by scanning electron microscope (SEM) (Figures 1g-i). An aligned CNT strand was observed at the healed "scar" to bridge the aligned CNTs from the two sides.

To quantitatively verify the efficient connection, the electrical resistances of the two fused composite films were investigated after fusing. They had been connected by two formats, i.e., "face to face" and "side by side", determined by the relative position of two films. The CNT layer was placed face to face with an overlapped section to enable the connection of the conducting pathway in a "face to face" fusion (Figure 2a), while

the two composite films were placed with the CNT and SHP layer being parallel with each other in a "side by side" fusion (Figure 2b). The electrical resistances were slightly increased by 4.6% and 7.6% after the "face to face" and "side by side" fusions compared with the total resistances of two composite films, respectively. The resistance variations were varied below 7% and 24% for the face-to-face and side-by-side fused film under bending, respectively, indicating a high flexibility (Figure 2c).

The fusible supercapacitor can be fabricated based on the aligned CNT/SHP composite films as two electrodes (Figure S5). Typically, poly (vinyl alcohol)-H_3PO_4 gel electrolyte was coated on the composite film, and the two electrodes were faced together. A key and different design in the two electrodes was conducted to realize the fusible functionality. The conducting CNT sheet was left blank without coating the gel electrolyte at three edges of an electrode, while one edge was left free of the gel electrolyte at the other electrode. The above design realized the access of in series or parallel connection of different units, as well as a close contact between different electrodes (Figure S6).

Carbon materials, such as activated carbon, carbon fiber (carbon cloth), CNT and graphene, have been widely investigated to fabricate flexible energy storage devices.[10-16] For instance, carbon clothes are used as conducting substrates to fabricate flexible supercapacitors. However, the resulting devices generally demonstrate low specific capacitances due to a low specific surface area and generally require functionality or modification to enhance device performances.[2b] To this end, carbon nanomaterials with much higher specific surface areas show better electrochemical performances. For example, the electrodes on the basis of multi-walled CNT exhibited a specific capacitance of 6.5 F g^{-1},[10] and chemically reduced graphene using hydrazine hydrate can produce high specific capacitances of 135 and 99 F g^{-1} in aqueous and organic electrolytes, respectively.[11] The further enhancement in the energy storage performance may be achieved by introducing conducting polymers or metal oxides.[15]

The dependence of the capacitive performances on CNT thickness was first explored. The galvanostatic charge-discharge curves were compared by increasing the CNT thickness from 80, 160 and 240 to 320 nm at the same current density of 0.15 A g^{-1} (Figure S7a). They shared a shape of symmetric triangle that indicated a high reversibility during the charge-discharge process. The specific capacitances were first increased from 10.39 to 15.68 F g^{-1} at increasing thicknesses from 80 to 240 nm due to the decreased resistance and then started to reduce with the further increase in the thickness, e.g., 13.65 F g^{-1} at 320 nm due to the less effective penetration of gel electrolyte in thicker CNT sheets (Figure S7b), which was confirmed in the Nyquist plots (Figure S8). The charge transfer resistance (R_{ct}) displayed a slight increase with

the increasing thickness of CNT sheets (inserted image in Figure S8). This phenomenon may be attributed to the fact that a thicker CNT sheet impedes the ion diffusion and migration process due to the hydrophobic nature of CNT.[14] The equivalent series resistance showed a decreasing trend from 315 to 200 Ohm with the increasing thicknesses of CNT sheets from 160 to 240 nm; it was slightly decreased to 180 Ohm when the thickness was further increased to 320 nm. The reason lies that the electrical resistance of the electrode was decreased with the increasing CNT thickness. Therefore, the CNT thickness of 240 nm was mainly studied below.

The electrochemical properties of invidual supercapacitors were firstly investigated. With increasing current densities from 0.15 to 1.50 A g^{-1}, the symmetric triangle shape of the galvanostatic charge-discharge curves had been well maintained, indicating a high electrochemical reversibility during charge-discharge processes (Figure S7c). At increasing scan rates of 200, 500 and 1000 mV s^{-1}, the rectangle shapes of CV curves further showed the excellent electrochemical stability (Figure S7d). The high cyclic stability was verified by low specific capacitances variation (below 4.5%) after 10000 charge-discharge cycles (Figure S7e).

The energy storage performances can be further enhanced by introducing active materials with pseudocapacitances such as conducting polymers and metal oxides. Polyaniline (PANI) was herein deposited onto aligned CNT sheets as a demonstration (Figure S9). The performances of supercapacitors based on bare CNT and CNT/PANI (PANI weight percentage of 70%) composite films were compared at the same current density of 0.75 A g^{-1} (Figure S7f). Large improvement on the specific capacitance of 185.2 F g^{-1} was obtained based on composite films, nearly 12 times higher than the bare CNT. A high reversibility during charge-discharge processes had been also observed for the CNT/PANI composite electrode at increasing current densities from 0.45 to 4.50 A g^{-1} (Figure S10). Satisfactory energy/power densities were achieved (6.82 Wh kg^{-1} at 225 W kg^{-1} and 2.48 Wh kg^{-1} at 2250 W kg^{-1}) (Figure S11) and are comparable to previously reported flexible supercapacitors based on carbon and conductive polymer materials, e.g., ~5.5 Wh kg^{-1} at ~264 W kg^{-1} based on CNT/PANI composite electrode[10] and ~ 4.6 Wh kg^{-1} at ~27.5 W kg^{-1} based on graphite/graphene/PANI composite electrode (on the basis of the total mass of the electrode).[17] The specific capacitances had been further maintained by 88.5% after 2000 charge-discharge cycles (Figure S12).

These supercapacitors can be connected at the edges of two neighboring electrodes, and a gentle pressing at the joint section fused them into one device through the self-healing of SHP. Because it was available to make a joint from any edge, these supercapacitors could be assembled into various patterns via different connection formats. As a demonstration, Figure 2d demonstrated the in-series connection in a face-to-face format.

With the joint edges being fused together, the patterned supercapacitor remained stable without fatigues in structure under twisting (Figure 2e). To further verify the high stability of the fused supercapacitor pattern, the galvanostatic charge-discharge and CV curves of the building supercapacitors had been compared before and after twisting. The curves were overlapped for both kinds of curves, with the specific discharge capacitances varied by only 1.9% (Figure 2f and Figure S13). The same high and stable electrochemical performance had been also verified after the incorporation of PANI (Figures S14, S15). Besides twisting, it was also important to investigate the stability under bending. Figures 2g, 2h showed the in-series pattern under bending, and the galvanostatic charge-discharge curves were almost identical under increasing bending angles from 0 °to 135 °(Figure 2i). More complex patterns could be produced according to this method, e.g., five supercapacitors were connected into a cross-shaped pattern by both in parallel and series connections (Figure 2j). Satisfactorily, the pattern remained stable with increasing twisting angles from 0 ° to 135 °, and the discharging time was fluctuated below 5% (Figures 2k, 2l).

It is simple and effective to vary the output voltages or currents from the fusible supercapacitors. Eight supercapacitors were fused in two formats (Figures 3a-c) to tune the working voltage as 3.2 or 6.4 V (Figure 3d). By fusing two more supercapacitors into the module (Figures 3e-g), the working voltages were increased to 4 and 8 V, respectively (Figure 3h). More complex patterns can be designed with twelve supercapacitors (Figures 3i-k). Although the working voltage was the same for the fused supercapacitors in Figures 3b and 3i, the latter showed an increased discharging time by 28% compared with the former under the same current as more units were connected in parallel. Under an ideal situation, it is calculated to be enhanced by 33% (see Supporting Information), which verifies the effective fusion among neighboring supercapacitors.

Perovskite solar cells have been widely studied as the next-generation photovoltaic device due to the combined high power conversion efficiency and all-solid-state structure which are particularly favorable for flexible electronics.[18-24] The above composite films had been also used to fabricate efficient perovskite solar cells with a fusible property (Figures 4a, b). Briefly, indium tin oxide coated on polyethylene naphthalate had been sequentially spin-coated with TiO_2, $CH_3NH_3PbI_3$ and Spiro-OMeTAD (detailed at the Experimental Section section), and a composite film typically with CNT thickness of 320 nm was closely attached onto the Spiro-OMeTAD layer serving as a back contact electrode to complete a fusible perovskite solar cell.[25,26] The high electrical conductivity of the aligned CNT sheet offered both high charge extraction and transport with short-circuit current density, open-circuit voltage and fill

factor of 15.30 mA cm^{-2}, 1.06 V and 0.48, respectively, which produced a power conversion efficiency of 7.80% (Figure 4c). As all components were flexible, the resulting perovskite solar cell was also flexible (Figure S16).

The same two fusible perovskite solar cells were fused into one in series by connecting the composite electrode from one device with the indium tin oxide electrode from the other device under mild pressing (Figure 4d, e). The short-circuit current was slightly decreased by 6.4% while the open-circuit voltage had been doubled to 1.90 V (Figure 4f). Of course, these fusible perovskite solar cells can be fused into various patterns, depending on the specific application. For instance, five perovskite solar cells were fused into one in series to increase the output voltage (Figure S17).

It is highly desired to simultaneously realize energy harvesting and storage in a single device.[27,28] Fusible supercapacitors and perovskite solar cells had been also fused into an integrated device by connecting the composite electrode from a supercapacitor with the composite electrode from a perovskite solar cell (Figure 4g). A switch was connected with the other two electrodes to control the photocharging and discharging processes. Under illustration, photovoltaic conversion was performed at the solar cell part, and the generated electric energy was stored in the supercapacitor when the switch was turned on. The photocharging process was terminated when the switch was turned off, and the charged supercapacitor can be then used to power an electronic device (Figure 4h). The energy storage efficiency ($\eta_{storage}$) and entire photovoltaic conversion and energy storage efficiency (η) were calculated from the following equations.

$$\eta_{storage} = \frac{\int UdQ}{E_{in}\eta_{conver}} = \frac{0.5\, It_{discharge}(U_2 - U_1)}{P_{in}t_{charge}S\,\eta_{conver}} \quad (1)$$

$$\eta = \frac{\int UdQ}{E_{in}} = \frac{0.5\, It_{discharge}(U_2 - U_1)}{P_{in}t_{charge}S} \quad (2)$$

Here Q is the charge during galvanostatic discharging process; E_{in} and η_{conver} are the incident solar energy and energy conversion efficiency of the perovskite solar cell, respectively; I and $t_{discharge}$ are the galvanostatic discharging current and time, respectively; U_1 and U_2 are the lowest and highest voltage, respectively; P_{in} is the illuminated light-energy density of 100 mW cm^{-2}; S and t_{charge} are the effective area of the solar cell and photocharging time, respectively. The maximal $\eta_{storage}$ and η were found to be 72.1% and 4.3%, respectively. The output voltages and capacitances could

be further controlled by varying the building units. The photocharging and discharging curves were similar, but the discharging voltages were 1.82 and 3.65 V for four and eight units, respectively (Figure S18). The integrated devices can stably discharge with increasing current densities (Figure 4i).

It should be noted that although this work mainly focuses a novel connection method for energy devices, the high device performance and efficient connection are largely dependent on the remarkable properties of used materials. For instance, aligned CNT sheets that are highly conductive not only serve as an excellent electrode material and framework for PANI but enable an electrically fusible process with the assistance of self-healing polymer; self-healing polymer has determined the structural connection and offers the connection of conductive networks; electrochemically deposited PANI enhances the energy storage performance of the device. Without the featured functions of the above materials, the novel connection and high performance cannot be obtained. More efforts are on the way to further enhance the device performance by optimizing the material structure and fabrication process.

Conclusions

To summarize, a new family of fusible energy harvesting and storage devices has been developed as basic building units to produce flexible, integrated powering systems. Compared with the traditional connection by external conducting wires, these fusible energy devices can be fused into various patterns at room temperature with high stability, high efficiency and low cost. In particular, they are assembled into desired patterns without complex templates and tedious fabrications, which remains difficult for the current technologies while becomes critical in many fields such as the portable and wearable electronics. The novel design on material and structure may represent a general and efficient strategy in the advancement of energy devices that require simple and efficient connections.

Experimental Section

The synthesis of SHP is described in the Supporting Information.[29,30] An polymer/chloroform solution (0.1 g mL^{-1}) was drop-casted onto clean glass slides to produce thin films. Aligned CNT sheets were drawn from spinnable CNT arrays synthesized by chemical vapor deposition with a height of 200 μm (Figure S3).[8,9] The aligned CNT sheets (thickness of ~20 nm for a single layer) were orthogonally overlapped onto a SHP film.

To fabricate supercapacitors, the aligned CNT/SHP composite film was cut into two different sizes of 10×8 or 8×6 mm and served as electrodes. The effective area of each supercapacitor was 6×6 mm, and the touched edge shared a width of ~2 mm. 0.1 M aniline and 1.0 M H_2SO_4 were used as the electrolyte to perform the electro-polymerization at 0.75 V vs. SCE. The calculation of PANI mass was previously reported.[10] PANI weight percentage of 70% was investigated. For the CNT thickness of 240 nm, the loading PANI density was 39.5 μg cm^{-2}. The poly (vinyl alcohol)-H_3PO_4 gel electrolyte with poly (vinyl alcohol) powder (1 g) in deionized water (9 mL) and H_3PO_4 (1 mL) was then coated on the film electrodes. The same two electrodes were assembled face to face after drying the gel electrolyte at room temperature for 4 h.

To fabricate a perovskite solar cell, indium tin oxide-coated polyethylene naphthalate flexible substrate was sequentially washed with acetone, isopropanol and deionized water under ultrasonic bath. TiO_2 nanoparticles dispersed in ethanol were spin-coated onto the treated substrate at a rotation speed of 5000 rpm for 30 s. A layer of PbI_2 was further deposited at a rotation speed of 4000 rpm for 30 s and dried at 80 ^oC for 30 min. After cooled down to room temperature, the resulting substrate was dipped into a CH_3NH_3I/isopropanol solution (10 mg mL^{-1}) for 30 s and annealed at 80 ^oC for 30 min, followed by coating the Spiro-OMeTAD hole transport layer (61.4 mM of 2,2',7,7'-tetrakis (N,N-di-p-methoxyphenylamine)-9,9-spirobifluorene, 26 mM of lithium bis(trifluoromethylsulfonyl) imide and 55 mM of 4-tert-butylpyridine in a mixed solvent of chlorobenzene and acetonitrile with a volume ratio of 20/1) at a rotation speed of 3000 rpm for 60 s. A CNT/SHP composite film with CNT thickness of 320 nm was directly attached onto the hole transport layer to obtain the perovskite solar cell. The perovskite solar cell and supercapacitor were integrated into a single one by attaching their composite electrodes together.

The structures and morphologies were characterized by scanning electron microscopy (Hitachi FE-SEM S-4800 operated at 1 kV) and optical microscopy (Olympus BX51). The electrical resistances were measured on a Keithley Model 2400 Source Meter. The cyclic voltammogram, galvanostatic charge-discharge curves and electro-polymerization were conducted at an electrochemical workstation (CHI 660a). The cyclic charge-discharge measurement was performed on an Arbin multi-channel electro-chemical testing system (Arbin, MSTAT-5 V/10 mA/16 Ch). The J-V curves were obtained by a Keithley 2420 Source Meter under illumination (100 mW cm^{-2}) of simulated AM1.5 solar light derived from a solar simulator (Oriel-Sol3A 94023A equipped with a 450 W Xe lamp and an AM1.5 filter). The specific capacitance (C) of the electrode was calculated from the equation of $C_{electrode} = 2\times(I\times\Delta t)/(\Delta V\times m)$, where I, Δt, ΔV and m correspond to discharge current, discharge time, voltage variation and mass of active material on one electrode, respectively.[10,31] The photocharge and

galvanostatic discharge curves were measured at an electrochemical workstation (CHI 660a) under illumination (100 mW cm^{-2}).

Acknowledgements

The authors acknowledge funding support from MOST (2011CB932503), NSFC (21225417), STCSM (12nm0503200), the Fok Ying Tong Education Foundation, the Program for Special Appointments of Professors at Shanghai Institutions of Higher Learning, and the Program for Outstanding Young Scholars from the Organization Department of the CPC Central Committee.

References

1 a) Y. Meng, Y. Zhao, C. Hu, H. Cheng, Y. Hu, Z. Zhang, G. Shi, L. Qu, *Adv. Mater.* **2013**, *25*, 2326. b) Y. Zhao, J. Liu, Y. Hu, H. Cheng, C. Hu, C. Jiang, L. Jiang, A. Cao, L. Qu, *Adv. Mater.* **2013**, *25*, 591. c) C. Hu, G. Zheng, F. Zhao, H. Shao, Z. Zhang, N. Chen, L. Jiang, L. Qu, *Energy Environ. Sci.* **2014**, *7*, 3699.

2 a) J. Xu, M. Wang, N. P. Wickramaratne, M. Jaroniec, S. Dou, L. Dai, *Adv. Mater.* **2015**, DOI: 10.1002/adma.201405370. b) M. Yu, Y. Zeng, C. Zhang, X. Lu, C. Zeng, C. Yao, Y. Yang, Y. Tong, *Nanoscale* **2013**, *5*, 10806. c) D. S. Yu, K. Goh, H. Wang, L. Wei, W. C. Jiang, Q. Zhang, L. M. Dai, Y. Chen, *Nat. Nanotechnol.* **2014**, *9*, 555. c) T. Chen, Y. H. Xue, A. K. Roy, L. M. Dai, *ACS Nano* **2014**, *8*, 1039.

3 a) M. Yu, Y. Zhang, Y. Zeng, M.-S. Balogun, K. Mai, Z. Zhang, X. Lu, Y. Tong, *Adv. Mater.* **2014**, *26*, 4724. b) Y. Zeng, Y. Han, Y. Zhao, Y. Zeng, M. Yu, Y. Liu, H. Tang, Y. Tong, X. Lu, *Adv. Energy Mater.* **2015,** 1402176.

4 H. Wang, B. Zhu, W. Jiang, Y. Yang, W. R. Leow, H. Wang, X. Chen, *Adv. Mater.* **2014**, *26*, 3638.

5 H. Sun, H. Li, X. You, Z. Yang, J. Deng, L. Qiu, H. Peng, *J. Mater. Chem. A* **2014**, *2*, 345-349.

6 H. Sun, Z. Yang, X. Chen, L. Qiu, X. You, P. Chen, H. Peng, *Angew. Chem. Int. Ed.* **2013**, *125*, 8434.

7 H. Sun, X. You, Y. Jiang, G. Guan, X. Fang, J. Deng, P. Chen, Y. Luo, H. Peng, *Angew. Chem. Int. Ed.* **2014**, *126*, 9680.

8 W. Wang, X. Sun, W. Wu, H. Peng, Y. Yu, *Angew. Chem. Int. Ed.* **2012**, *124*, 4722.

9 H. Sun, H. P. Li, X. You, Z. B. Yang, J. Deng, L. B. Qiu, H. S. Peng, *J. Mater. Chem. A* **2014**, *2*, 345.

10 H. Lin, L. Li, J. Ren, Z. Cai, L. Qiu, Z. Yang, H. Peng, *Sci. Rep.* **2013**, *3*, 1353.

11 M. Stoller, S. Park, Y. Zhu, J. An, R. Ruoff, *Nano Lett.* **2008**, *8*, 3498.

12 N. Li, Z. Chen, W. Ren, F. Li, H. Cheng, *Proc. Natl. Acad. Sci.* **2012**, *109*, 17360.

13 H. Gwon, H. Kim, K. Lee, D. Seo, Y. Park, Y. Lee, B. Ahn, K. Kang, *Energy Environ. Sci.* **2011**, *4*, 1277.

14 J. Liu, L. Zhang, H. Wu, J. Lin, Z. Shen, X. Lou, *Energy Environ. Sci.* **2014**, *7*, 3709.

15 J. Liu, J. Sun, L. Gao, *J. Phys. Chem. C* **2010**, *114*, 19614.

16 J. Liu, M. Chen, L. Zhang, J. Jiang, J. Yan, Y. Huang, J. Lin, H. Fan, Z. Shen, *Nano Lett.* **2014**, *14*, 7180.

17 G. Xin, Y. Wang, X. Liu, J. Zhang, Y. Wang, J. Huang, J. Zang, *Electrochim. Acta* **2015**, *167*, 254.

18 M. A. Green, A. Ho-Baillie, H. J. Snaith, *Nat. Photon.* **2014**, *8*, 506.

19 M. Liu, M. B. Johnston, H. J. Snaith, *Nature* **2013**, *501*, 395.

20 H. P. Zhou, Q. Chen, G. Li, S. Luo, T. B. Song, H. S. Duan, Z. R. Hong, J. B. You, Y. S. Liu, Y. Yang, *Science* **2014**, *345*, 542.

21 J. Burschka, N. Pellet, S.-J. Moon, R. Humphry-Baker, P. Gao, M. K. Nazeeruddin, M. Gratzel, *Nature* **2013**, *499*, 316.

22 J.-H. Im, I.-H. Jang, N. Pellet, M. Grätzel, N.-G. Park, *Nat. Nanotechnol.* **2014**, *9*, 927.

23 N. J. Jeon, J. H. Noh, Y. C. Kim, W. S. Yang, S. Ryu, S. I. Seok, *Nat. Mater.* **2014**, *13*, 897.

24 J. H. Heo, S. H. Im, J. H. Noh, T. N. Mandal, C.-S. Lim, J. A. Chang, Y. H. Lee, H.-j. Kim, A. Sarkar, K. NazeeruddinMd, M. Gratzel, S. I. Seok, *Nat. Photon.* **2013**, *7*, 486.

25 Z. Li, S. A. Kulkarni, P. P. Boix, E. Z. Shi, A. Y. Cao, K. W. Fu, S. K. Batabyal, J. Zhang, Q. H. Xiong, L. H. Wong, N. Mathews, S. G. Mhaisalkar, *ACS Nano* **2014**, *8*, 6797.

26 S. N. Habisreutinger, T. Leijtens, G. E. Eperon, S. D. Stranks, R. J. Nicholas, H. J. Snaith, *Nano Lett.* **2014**, *14*, 5561.

27 T. Chen, L. Qiu, Z. Yang, Z. Cai, J. Ren, H. Li, H. Lin, X. Sun, H. Peng, *Angew. Chem. Int. Ed.* **2012**, *51*, 11977.

28 Z. Yang, L. Li, Y. Luo, R. He, L. Qiu, H. Lin, H. Peng, *J. Mater. Chem. A* **2013**, *1*, 954.

29 P. Cordier, F. Tournilhac, C. Souli é-Ziakovic, L. Leibler, *Nature* **2008**, *451*, 977.

30 B. C. Tee, C. Wang, R. Allen, Z. Bao, *Nat. Nanotechnol.* **2012**, *7*, 825.

31 H. Sun, X. You, J. Deng, X. Chen, Z. Yang, J. Ren, H. Peng, *Adv. Mater.* **2014**, *26*, 2868.

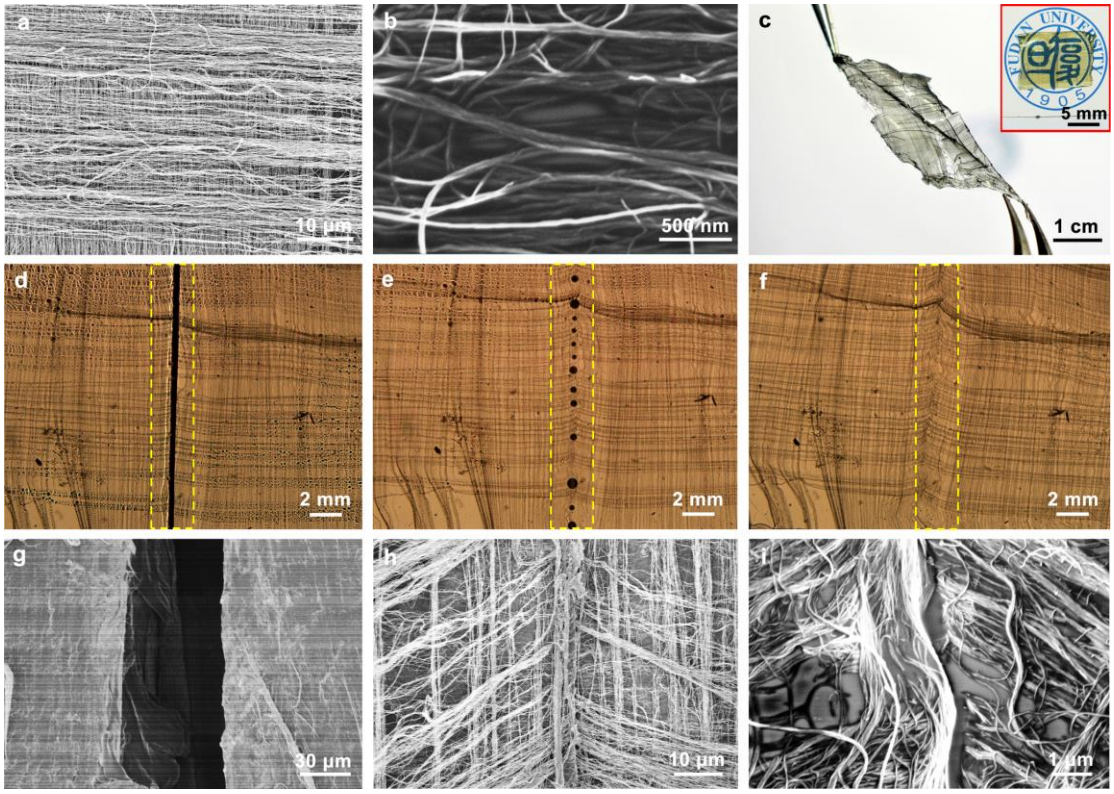

Figure 1. **a, b**. Scanning electron microscopy (SEM) images of an aligned CNT/SHP composite film at low and high magnifications, respectively. **c**. Photograph of a fused composite film. The inserted image showed the composite film at a labelled paper. Scale bar, 5 mm. **d-i**. Fusing process of the composite film traced by optical microscopy (**d-f**) and SEM (**g-i**). The labelled retangles by dashed yellow lines at (**d-f**) correspond to the fused area.

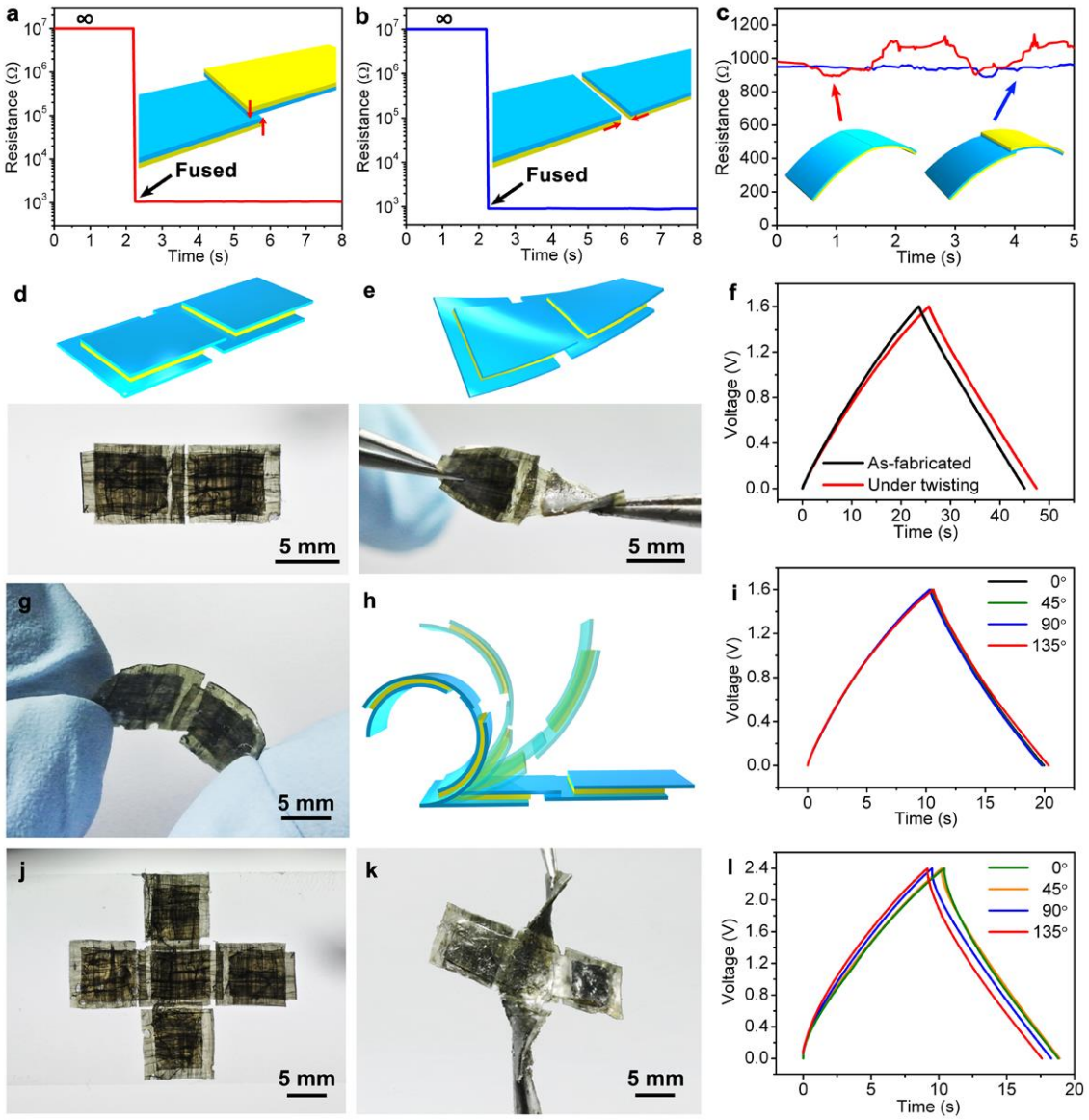

Figure 2. **a, b**. Resistance variations of two CNT/SHP composite films (20×8 mm) before and after fusing through face-to-face and side-by-side formats, respectively. The inserted scheme indicated the connecting process. **c**) Resistance variations of two CNT/SHP composite films (20×8 mm) connected by face to face and side by side under bending. **d-f**. Schematic illustration, photograph and galvanostatic charge-discharge curves of two fusible supercapacitors fused in series before and after twisting, respectively. **g-i**. Photograph, schematic illustration and galvanostatic charge-discharge curves (with increasing bending angles from 0 to 135 °) of two fused supercapacitors under bending, respectively. **j-l**. Photographs (**j, k**) and galvanostatic charge-discharge curves (**l**) (with increasing twisting angles from 0 to 135 °) of five fused supercapacitors under twisting. The current densities are 0.15 A g^{-1} at (**f**) and 0.30 A g^{-1} at (**i**), and the current at (**l**) is the same to (**i**).

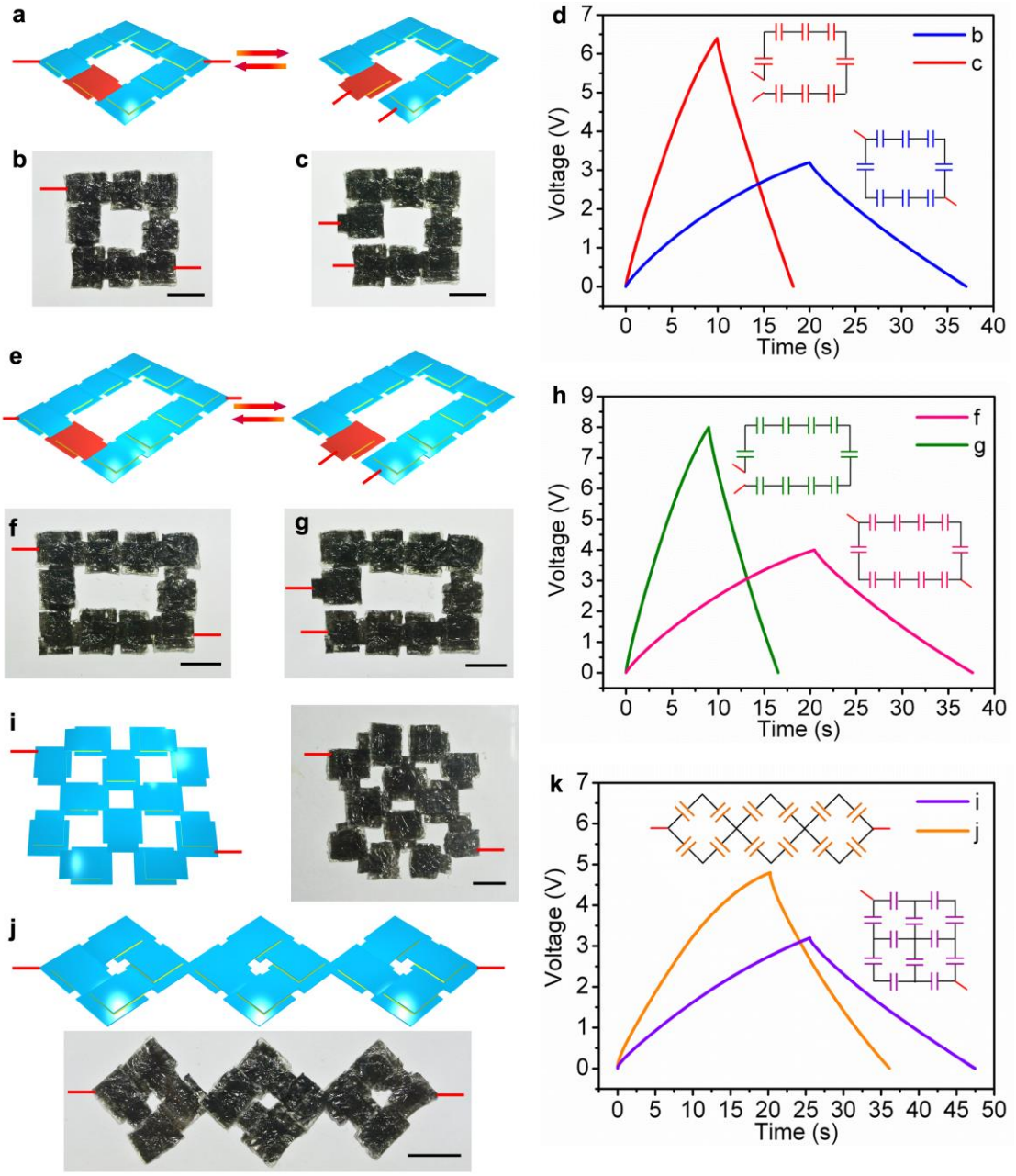

Figure 3. **a**. Schematic illustration to two kinds of connections for eight supercapacitors. **b-d**. Photographs (**b, c**) and galvanostatic charge-discharge curves (**d**) of the fused supercapacitors at (**a**). **e**. Schematic illustration to two kinds of connections for ten supercapacitors. **f-h**. Photographs (**f, g**) and galvanostatic charge-discharge curves (**h**) at (**e**). **i, j**. Schematic illustrations and photographs for twelve supercapacitors fused by different formats. **k**. Galvanostatic charge-discharge curves of the fused supercapacitors at (**i**) and (**l**). The inserted images at (**d**), (**h**) and (**k**) show the equivalent circuit of corresponding curves at the same charge-discharge current. Scale bar, 1 cm.

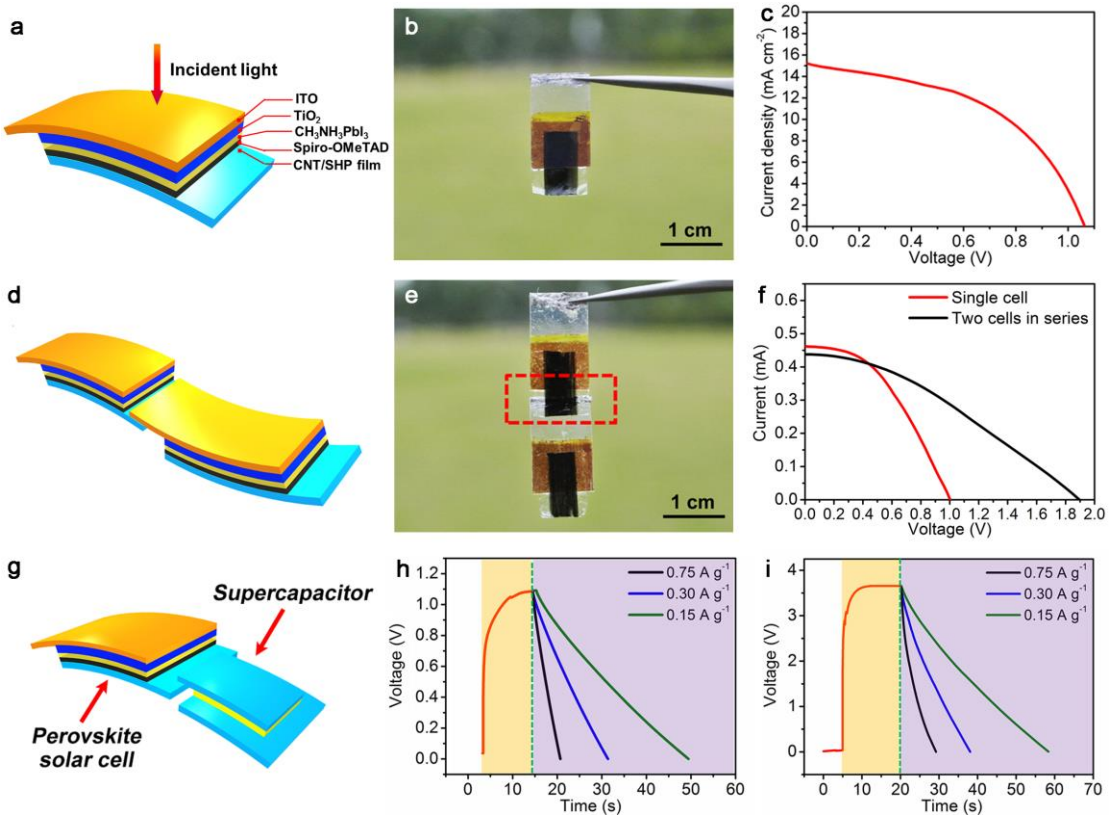

Figure 4. Fused perovskite solar cells and integrated devices. **a, b**. Schematic illustration and photograph of a fusible perovskite solar cell, respectively. **c**. J-V curve of a fusible perovskite solar cell. **d, e**. Schematic illustration and photograph of two fusible perovskite solar cells being fused in series. **f**. Current-voltage curves of individual and two fused perovskite solar cells. **g, h**. Schematic illustration and photocharging and galvanostatic discharging curves of the integrated device composed of a supercapacitor and a perovskite solar cell, respectively. **i**. Photocharging and galvanostatic discharging curves of the integrated eight units with increasing discharging current densities. The yellow and purple areas in (**h**) and (**i**) correspond to the photocharging and discharging processes, respectively.

The Table of Contents

Novel integrated energy harvesting and storage devices that can be jointed and fused into various patterns at room temperature are developed by simply stacking and gently pressing supercapacitors and perovskite solar cells. A wide variety of flexible device patterns can be designed and formed through the fusing process in either series or parallel connection or both to satisfy a broad spectrum of applications.